Hindawi
Shock and Vibration
Volume 2017, Article ID 3754510, 17 pages
https://doi.org/10.1155/2017/3754510

Research Article

Incremental Explosive Analysis and Its Application to Performance-Based Assessment of Stiffened and Unstiffened Cylindrical Shells Subjected to Underwater Explosion

Masoud Biglarkhani[1] and Keyvan Sadeghi[2]

[1]*Department of Civil Engineering, Hormozgan University, Bandar Abbas 3995, Iran*
[2]*Department of Mechanical Engineering, Buein Zahra Technical University, Qazvin 3451745346, Iran*

Correspondence should be addressed to Keyvan Sadeghi; keyvan.sadeghi@bzte.ac.ir

Received 26 April 2017; Accepted 24 September 2017; Published 31 October 2017

Academic Editor: Yuri S. Karinski

Incremental explosive analysis (IEA) is addressed as an applicable method for performance-based assessment of stiffened and unstiffened cylindrical shells subjected to underwater explosion (UNDEX) loading. In fact, this method is inspired by the incremental dynamic analysis (IDA) which is a known parametric analysis method in the field of earthquake engineering. This paper aims to introduce the application of IEA approach in UNDEX in order to estimate different limit states and deterministic assessment of cylindrical shells, considering the uncertainty of loading conditions. The local, bay, and general buckling modes are defined as limit states for performance calculation. Different standoff distances and depth parameters combining several loading conditions are considered. The explosive loading intensity is specified and scaled in several levels to force the structure through the entire range of its behavior. The results are plotted in terms of a damage measure (DM) versus selected intensity measure (IM). The statistical treatment of the obtained multi-IEA curves is performed to summarize the results in a predictive mode. Finally, the fragility curves as damage probability indicators of shells in UNDEX loading are extracted. Results show that the IEA is a promising method for performance-based assessment of cylindrical shells subjected to UNDEX loading.

1. Introduction

Cylindrical shells play a main role as basic structural elements in the construction of marine and submarine structures. Their relatively high stability against lateral pressure makes them a suitable choice for submerged pressure vessels and structures such as submarines and platform piles. There are numerous threats that can jeopardize cylindrical shells' performance subjected to underwater dynamic loadings that are associated with rigorous nonlinearities, where the water incompressibility and inertial characteristics make these affects more elaborate. Among different dynamic loadings, UNDEX has special importance in designing marine structures. The explosion itself involves several nonlinearities, which is related to very intense and rapid energy conversion phenomena; when this property is combined with water inherent characteristics, UNDEX and its effect on structures become an intricate problem. Therefore, experimental studies play an important role in the extraction of design and analysis points in UNDEX related problems, but due to the very expensive and dangerous essence of these types of tests, they are confined to scaled-down specimens and limited in the variation of parameters. Nevertheless, real scale tests have been conducted under classified programs in some countries, but their data are rarely published. On the other hand, by careful implementation of numerical simulations, valuable results can be obtained by much lower costs compared to experiments. Numerical procedures, if implemented correctly, can be very efficient for studying UNDEX problems, where related parameters must be varied in an extended range. There is a considerable amount of research concerned with the response of structures subjected to the UNDEX. Both experimental and numerical methods are implemented in these studies. As can be expected, analytical methods

can be applied to the oversimplified models and are not suitable for accurate analysis of UNDEX problems. Published works related to the UNDEX response of cylindrical shells are fewer than those related to plates and planar objects. Kwon and Fox [1] reported their numerical and experimental results in which 27.3 kg of HBX-1 explosive in 7.62 m standoff made a side-on shock on an aluminum cylinder. The problem was simulated in VEC/DYNA3D code and numerical results were in good agreement with experiments. In a pure experimental study, Brett et al. [2] investigated near-field explosion effect on mild steel cylindrical shells. Ramajeyathilagam et al. [3] investigated cylindrical shell panels subjected to underwater explosion loading experimentally and numerically. They implemented different span ratios of air-backed panels. CSA/GENSA (DYNA3D) was employed to simulate the process, and high strain rate effect and material and geometrical nonlinarites were also included in the analysis. Zhang and Yang [4] presented a spline shell element suitable for the dynamic response of submerged structures. Their proposed element had C^1 continuity and showed good performance in modeling underwater loadings. The implosion of cylindrical shells subjected to dynamic lateral hydrostatic pressure has been investigated by Gish [5]. Hsu et al. [6] made a comparison between various empirical formulas for application of shock-induced pressure on cylindrical shells with numerical models. Their reference for judgment on the accuracy of different formulations was the experimental results of [1]. Hung et al. [7], using the USA/DYNA package, simulated an UNDEX experiment and compared its results with test results. They used doubly asymptotic approximation (DAA) formulation and empirical formulas for prediction of shock loading and found relatively good correlation between tests and numerical results. Also, Xiao et al. [8] studied the whipping response of a fluid-filled structure subjected to underwater explosion by doubly asymptotic approximation and finite element method using ABAQUS and validated numerical results with analytical solutions. Lee et al. [9] simulated the German HDW U209-1400 submarine and studied the effect of shock wave generated by underwater explosion caused by a torpedo's detonation near the pressure hull and the response of the cylindrical structure analyzed by implementing ABAQUS Underwater Shock Analysis codes. Jen [10] used ABAQUS acoustic capability for UNDEX modeling and by an extended interior penalty function method optimized stiffening configuration of a submerged cylindrical capsule exposed to shock loading. Gupta et al. [11] experimentally investigated the mechanism of dynamic buckling instability that occurred in cylindrical structures subjected to underwater explosion. They conducted experiments with different load conditions by varying the pressure pulse and the hydrostatic pressure induced on the structure to determine the threshold followed by a particular dynamic buckling mechanism. Yin et al. [12] studied the response of both bare and coated hulls subjected to underwater explosion loading and considered the shock wave effects on the structure as well as hydrostatic pressure. They also focused on the shock mitigation effect of the coating on the hull wall. Li and Rong [13] conducted underwater explosion experiments on an aluminum cylinder and used MSC.DYTRAN code for the numerical simulation. The effect of geometrical imperfections on the UNDEX damage response of stiffened and unstiffened cylindrical shells was investigated numerically by Shin and Hooker [14]. Yao et al. [15] suggested a new shock factor useful for assessment of double stiffened cylindrical shells' response in UNDEX loading. Their modeling was established in ABAQUS environment. Zhang and Jiang [16] introduced an improved shock factor for small structures in comparison to the wavelength of the incident shock wave. They utilized the coupled mode method to investigate the scattering field surrounding the cylindrical shells. Ring-stiffened cylinders are very useful in reinforcing shells in marine applications. Dynamic response of this type of structures subjected to UNDEX loading in various depths is scrutinized by Yuan and Zhu [17] using numerical studies in MSC.DYTRAN. Explosive loading has an innate uncertainty which returns to its dependency on standoff distance and amount of explosive charge. Other uncertainty sources can be the position and attack angle of the shock wave. The aforementioned list can be extended further to include depth, variable density, and salinity of the water. Researches concerning this fact are rare and published data can rarely be found in this field. In recent decades, some efforts have been made to cover the effect of loading uncertainty in the design and analysis of structures. To the best of the authors' knowledge, there is no research about the effect of combination of depth and standoff factors on the response of cylindrical shells with and without stiffeners subjected to UNDEX loading. Most of the researches concerning this subject are confined to a fixed standoff distance and the variation of depth parameter is also neglected in most studies. However, changing depth parameter is more challenging than the standoff distance because it requires substantially very deep UNDEX testing pools which are not available in most conventional test centers. This problem can be overcome by an indirect simulation of the depth parameter effect via the average hydrostatic pressure of the surrounding medium. Considering the amount of computational time that is required for accurate simulation of one UNDEX loading, it may seem that simulating a large number of loading conditions including combinations of depth and standoff parameters is a laborious task. To make it feasible, a limited number of loading conditions are simulated such that a wide spectrum of depth and standoff parameters can be covered, and then statistical methods are used to present and interpret simulation results for cylindrical shells. This procedure is called incremental explosive analysis (IEA). It is shown that IEA can be a reliable method for prediction of the dynamic behavior of cylindrical shells from a stable condition to unstable and finally the collapse states. The IEA can be employed in the design and/or assessment of marine structures subjected to UNDEX loading. In fact, it can use different performance levels or limit states and evaluate ultimate capacity of shells by using nonlinear dynamic explosive analyses. A relatively similar concept called incremental dynamic analysis (IDA) has been established in recent years in order to assess the performance of the building and fixed offshore structures subjected to seismic loading (see, e.g., [18–25]). Mansouri et al. [26] implemented the IDA method

on several-story buildings to analyze the damping effect of the lead-rubber bearing on the seismic performance of base isolated structures and represented the fragility curves to study the annual exceedance probability of some limit states. Based on the IDA, relatively novel methodologies have been proposed by some researchers for environmental loads other than earthquakes, such as Incremental Wave Analysis (IWA), Endurance Wave Analysis (EWA), and Incremental Wind Wave Analysis (IWWA) (Golafshani et al. [27], Zeinoddini [28]). In the present work, the dynamic response of stiffened and unstiffened submerged cylindrical shells under UNDEX loading is investigated by the proposed IEA method in a wide range of deformation modes. In this approach, by using various combinations of major factors in UNDEX such as charge depth and standoff distance, different loading conditions are generated. The inverse of the well-known scaled distance Z is chosen as the intensity measure (IM) and the peak of the deflection time history and the effective strain of cylinders are chosen as the damage measures (DMs). The intensity of loading is scaled in several levels for every depth and standoff combination to force the structure through the entire range of its behavior which covers postbuckling and plastic deformation regions as well as elastic ranges. Numerical simulations are performed in AUTODYN hydrocode environment and rigorous coupled Eulerian-Lagrangian models are implemented for this purpose. The target response is obtained and recorded for a particular intensity measurement and for every loading condition. Then, the multi-IEA curves are derived from several simulation results by direct postprocessing. According to the nonlinear part of the shells' response that covers postbuckling and plastic deformation of structures, three limit states, that is, bay buckling, local buckling, and general buckling, are defined. The statistical treatment of the obtained multi-IEA curves is performed to summarize the results and to use them effectively in a predictive mode as a large amount of data is gathered. The cross-sectional fractiles method is used to summarize the extracted IEA curves. This will reduce the data to the distribution of DM given IM and to the probability of exceeding the defined limit states given the IM level. Finally, the fragility curves are derived as the damage indicator to acquire a design tool that provides useful information for quantitative damage analysis of shells in UNDEX loading. The IEA is implemented on four configurations of stiffened and unstiffened cylindrical shells with different thicknesses under different loading conditions.

2. Incremental Explosive Analysis

2.1. New Aspects of IEA. The entire range of cylindrical shells' behavior, from stable range to unstable and finally collapse of the system, and the deterministic assessment of structural performance are an important challenge for designers in UNDEX. Hence, innovative methods need to be proposed for the design and analysis of these types of structures to predicate the structural capacity and intuition of their behavior subjected to UNDEX loading. At first glance, UNDEX's effect on structures may appear as a simple problem. However, UNDEXs have some degree of uncertainty and complicacy where the two main parameters of depth and standoff distance have significant effects on the spatiotemporal distribution of impinging load on structures. These parameters are severely nonlinear and any attempt to find a concise relation covering all possible situations is an abortive task. As can be expected, there are countless loading conditions which can be created by the combination of depth and standoff factors. Evaluation of response of cylindrical shells subjected to numerous loading conditions is not an easy task and also is not practical. Hence, a limited number of loading conditions will be investigated by varying both the depth and the standoff distance parameters to extract an adequate level of information. Therefore, by considering the loading parameter of UNDEX and its effects on structures, the IEA is proposed in this study. The IEA involves performing multiple nonlinear dynamic analyses of a structural model of cylindrical shells under several levels of explosive intensity. The scaling levels are selected appropriately so as to force the shell structure through the entire range of its behavior. Then, appropriate postprocessing can generate the results in terms of IEA curves, one for each loading condition which is here a combination of standoff distance and depth parameter, of the explosive intensity, typically represented by a scalar intensity measure (IM), versus the structural response or demand. The structural response is identified as a damage measure (DM) and can be any structural response quantity that relates to structural damage. This method also enables checking for multiple performance levels or limit states. The objectives of this method include the following: (1) thorough understanding of the range of responses or "demands" versus the range of potential levels of an explosive intensity, (2) better understanding of the changes in the nature of the structural response as the intensity of explosive charge increases, (3) better understanding of the structural implications of rarer/more severe explosive intensity levels, (4) the estimation of structural dynamic capacity, and (5) finally the generation of multi-IEA curves indicating how variable (or stable) all these items are from one explosive intensity level to another.

2.2. Implementation of the IEA Procedure. Several steps are required for applying IEA on a structure in order to determine the performance of the structure, which are (1) generating a proper nonlinear structural model, (2) selection of suitable intensity measures (IM) and representative damage measures (DMs), (3) determining the scaling levels corresponding to IM, (4) employing proper interpolation, (5) estimation of the probability distribution of the structural demand given the explosive intensity by summarization techniques, and (6) definition of performance levels or limit states to calculate the corresponding capacities. Thus, in order to perform the IEA on a structure, at first, it is essential to define an intensity factor as a representative of the intensity of the applied loading condition. According to Cole [29], a well-known empirical-based parameter called the scaled distance is defined as

$$Z = \frac{R}{\sqrt[3]{W}}, \tag{1}$$

Table 1: Combination of various standoff distances (SD) and depth parameters (β).

SD (mm)	β (unstiffened shell)	β (stiffened shell)
300 (near)	7	7
600 (medium)	40	150
1000 (far)	90	300

where W is the equivalent TNT charge mass in kg and R is the standoff distance in meters measured from the center of the spherical charge to the location of the gauge point. Here, the inverse of the scaled distance is chosen as the intensity measurement parameter:

$$\mathrm{IM} = \frac{1}{Z} = \frac{\sqrt[3]{W}}{R}. \tag{2}$$

The standoff distance between the explosive and the structure and the depth of the explosion are the most dominant factors in UNDEX loading. The major effects of the depth parameter are related to the temporal variation of pressure, duration of UNDEX pulsations, and bubble migration [30]. Another main effect of the depth parameter is connected to the preloading of the structure due to the initial hydrostatic pressure. To better quantify this effect, a scaled depth parameter is implemented as follows [31]:

$$\beta = \frac{h}{\sqrt[3]{W}}, \tag{3}$$

where W is the equivalent TNT mass in kg and h is the depth in meters measured from the water surface. Nine combinations of the probable loading conditions are, therefore, considered here to take into account a wide range of possibilities. Table 1 represents the implemented (β, SD) loading conditions.

In the IEA, the IM values are going to be increased incrementally in such a way that the whole range of cylindrical shell responses is covered accordingly. It should be noted that an individual nonlinear Finite Element Analysis (FEA) is conducted for obtaining the structural response for every IM value of all nine combinations (β, SD). After an accurate definition of IM, it is required to define the damage measure (DM) parameter to indicate the structural response under distinct loading conditions and IMs. In this study, two different damage parameters are considered. First, the maximum rotation of cylindrical shell edge (θ) is considered, which is the ratio of the maximum deflection of the cylinder at its middle region to its half-length. Second, the ductility ratio is considered, which is defined as

$$\mu = \frac{\varepsilon_M}{\varepsilon_{El}}, \tag{4}$$

where ε_M and ε_{El} are the equivalent strain in the cylinder center and the maximum elastic strain, respectively. The incremental values for IM are provided in Section 5. Then, the IEA curves can be generated and pinned on the IM-DM plane for every combination of (β, SD) representing the structural responses for the different explosive masses and environmental factors. After extraction of the desired IM and DM values from each of the dynamic analyses, a set of discrete points are available for each combination of (β, SD) that reside in the IM-DM plane and lie on its IEA curve, as shown in Figure 1. By interpolating them, the entire IEA curve can be approximated and there will be no need to perform additional analyses. To do this, the superior spline interpolation as realistic interpolation is generated in order to accurately represent the real IEA curves.

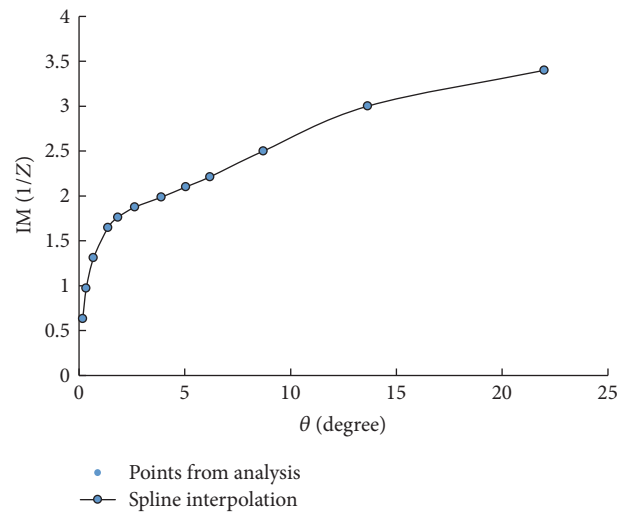

Figure 1: The obtained IM-DM points for (300, 7) for different IM values.

As mentioned previously, in order to attain proper damage measurement parameters, reliable limit states should be defined, representing the allowable load applied on the structure. Hence, choosing an appropriate limit state determines the validity and accuracy of the incremental damage study. Since the structures are too vulnerable to the buckling failure, the ductility ratio μ is also obtained for the conducted analysis to compare the maximum failure strain of the cylindrical shell material and the corresponding value of the equivalent strain at the general buckling mode. In the present study, three distinct limit states are represented for evaluating the performance of the stiffened and unstiffened cylindrical shells: bay buckling, local buckling, and general buckling. As suggested by ABS [32], a stiffened cylindrical shell should be considered in such a way that bay buckling precedes both local and general buckling. Bay buckling refers to buckling of shell plating together with the stringers, if present, between adjacent ring stiffeners. Bay buckling limit state for an unstiffened or ring-stiffened cylindrical shell subjected to external pressure, such as pressure waves of explosion, occurs when the external pressure reaches the critical value below:

$$\sigma = \Phi \sigma_{E\theta R}, \tag{5}$$

where Φ is the plasticity reduction factor and depends on the ratio between the elastic hoop buckling stress ($\sigma_{E\theta R}$) and the yield stress of an imperfect cylindrical shell material. The elastic hoop buckling stress ($\sigma_{E\theta R}$) depends on the stiffeners'

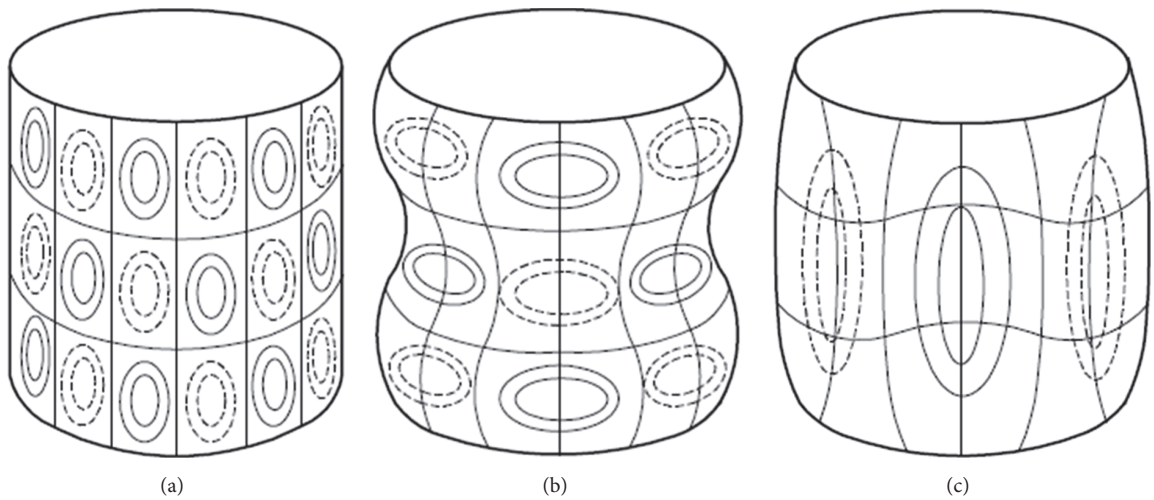

Figure 2: Three different limit state schematic representations: (a) local shell buckling, (b) bay buckling, and (c) general buckling [32].

layout, geometrical parameters of the cylindrical shell, and elasticity properties of the shell material. Further details are described in [32]. On the other hand, local shell buckling refers to buckling of the shell between adjacent stiffeners. Moreover, general buckling refers to buckling of one or more ring stiffeners together with the attached shell plus stringers. Figure 2 demonstrates the implemented distinct limit states in the present study.

After simulations are performed, a relatively large amount of data becomes available. Presentation of these data by multiple curve diagrams may be useful for a brief comparison of the effect of various parameters; however, they cannot be handled easily by a designer. To address this issue, an appropriate summarization technique is employed in order to reduce this data which provides indirect information about the probability of occurrence of an identical level of DM for every IM. In this study, the cross-sectional fractiles method is implemented for IEA curves summarization [33] and the capacities of the limit states are summarized into mean value and difference between two fractiles. To do so, the 16%, 50%, and 84% fractile values of DM ($DM^C_{16\%}$, $DM^C_{50\%}$, and $DM^C_{84\%}$, resp.) and IM ($IM^C_{16\%}$, $IM^C_{50\%}$, and $IM^C_{84\%}$, resp.) for each limit state are chosen to be calculated accordingly. More details about this method are discussed in Section 6. It is more advantageous to illustrate the abovementioned characteristics by fragility diagrams where the occurrence of various limit state probabilities can be extracted for every IM level. Most of the blast resistive structures are designed to tolerate extreme loading conditions where the probability of occurrence of these loadings is not similar to conventional threats and often an overestimated safety factor is considered in the design. These overestimations of parameters are crucial in underwater moving objects' designs where consumption of energy and weight optimization are determinative. In this regard, IEA curves can be a design tool for efficient design of stiffened cylindrical shells in explosion resistive marine structures.

3. Numerical Modeling Considerations

The effect of underwater explosion on structures is associated with many complicated nonlinear phenomena such as the interaction of solid boundary and inertial medium of water, very high loading rate of explosion, strain rate effects on material behavior, and large deformations. Hence, for precise design and analysis of structures subjected to UNDEX, experimental studies on reduced scale models are invaluable. On the other hand, most of the full-scale experimental tests are conducted under military programs and their data are classified. Another effective and powerful method is the numerical simulation if implemented accurately. Coupled numerical models can be used to simulate complicated fluid–structure interaction (FSI) problems in a feasible way. The rate of deformation of a fluid medium is very high in comparison with solid continua and this fact must be taken into account in modeling FSI UNDEX problems. The Eulerian approach in discretizing water medium and the ordinary nonlinear shell Lagrangian method are utilized to avoid numerical troubles that arise due to severe distortion of elements. Shell elements are assumed to be in full coupling with the surrounding fluid. To better capture the shock wave distribution in water, the explosion must be modeled from the beginning of detonation.

3.1. Governing FSI Equations. Numerous sources are available for details of finite element modeling and computational fluid dynamics. Lagrangian-Eulerian procedures are common to get feasible results from FSI UNDEX problems. The discretized differential equations of motion of the structure can be presented as follows [34]:

$$M\ddot{x} + C\dot{x} + Kx = F(t), \tag{6}$$

where M, C, and K are structural mass, damping, and stiffness matrices, respectively; x is the structural displacement vector; an overdot is used for differentiation with respect to

Table 2: JWL constants of TNT.

C_1 (GPa)	C_2 (GPa)	R_1	R_2	ω	ρ_0 (kg/m^3)
373.7	3.74	4.15	0.9	0.35	1630

time; and $F(t)$ is the force vector which is calculated according to the FSI algorithm. Superimposing the imaginary fluid mesh on the fluid–solid interface leads to the compatibility relation for submerged structures:

$$F(t) = -GA_f(p_i + p_s), \tag{7}$$

where p_i is the incident fluid pressure (here UNDEX overpressure and pulsations), p_s is the scattered pressure of the structure, G is a matrix that couples structural degrees of freedom to the fluid grid, and A_f is the matrix that stores information of areas of Lagrangian elements in fluid cells. A compatibility equation that enforces the fluid and structure surface grids to have the same normal velocity can be expressed as

$$G^T\dot{x} = \mu_i + \mu_s \tag{8}$$

in which the superscript T refers to matrix transposition, μ_i is the incident water particle velocity, and μ_s is the scattered water particle velocity induced by structural interactions.

3.2. Jones-Wilkins-Lee (JWL) Equation of State. Highly explosive detonative reactions are accompanied with a high amount of chemical energy conversion to heat and mechanical waves, which makes the exact modeling of the phenomenon by continuum assumption rather impossible. This energy conversion process, however, can be predicted with acceptable accuracy by Jones-Wilkins-Lee (JWL) equation of state (EoS) as follows:

$$P = C_1\left(1 - \frac{\omega}{R_1 v}\right)e^{-R_1 v} + C_2\left(1 - \frac{\omega}{R_2 v}\right)e^{-R_2 v} + \frac{\omega e}{v}, \tag{9}$$

where v is the specific volume of detonation products over the specific volume of undetonated explosive, e is the specific internal energy, and C_1, C_2, R_1, R_2, and ω are material constants and for TNT are given in Table 2 [35].

3.3. Equation of State of Water. Water as an incompressible fluid has a negligible strength and its dynamic behavior can be modeled with adequate accuracy using the definition of a polynomial equation of state (EoS). This EoS defines the pressure as

$$p = A_1\mu_d + A_2\mu_d^2 + A_3\mu_d^3 + (B_0 + B_1\mu_d)\rho_0 e \quad \text{for } \mu_d > 0 \ (\text{compression}) \tag{10}$$

$$p = T_1\mu_d + T_2\mu_d^2 + B_0\rho_0 e \quad \text{for } \mu_d < 0 \ (\text{Tensile}),$$

where $\mu_d = \rho/\rho_0 - 1$; ρ_0 is the initial density; A_1, A_2, A_3, B_0, B_1, T_1, and T_2 are constants that are presented in Table 3 [35]; and e is the internal energy per unit mass. The effect of depth can be accommodated in internal energy of water using the following relation:

$$e = \frac{\rho g h + p_0}{\rho B_0}, \tag{11}$$

where ρ is the density, h is the depth measured from the free surface of water, p_0 is the atmospheric pressure, and g is gravitational acceleration (9.81 m/s^2).

3.4. Equation of State of Air. The stiffened and unstiffened cylindrical shells studied in this article are air-backed in their inner side. Therefore, an EoS for modeling of air effect is needed. Typically ideal-gas EoS is sufficient for accurate results. This is defined by the ideal-gas gamma-law relation as follows:

$$p = (\gamma - 1)\frac{\rho}{\rho_0}E, \tag{12}$$

where E is the specific energy, γ is the ratio of the constant pressure over constant volume specific heat (=1.4 for air), ρ_0 is initial density (=1.225 × 10^{-3} g/cm^3), and ρ is current density. If standard air condition is specified, E must be set to 253.4 (kJ/m^3).

3.5. Johnson-Cook Strength Model for Steel. Usually, metals exhibit a strain rate sensitive behavior when subjected to high rate dynamic loading. Steel as the main material for construction of marine structures is considerably more sensitive to high rate dynamic loading in comparison with other metals. In most UNDEX loadings, strain rate can reach up to 10^4/s; hence, to get accurate results, an acceptable rate sensitive strength model must be used. The Johnson-Cook model can predict the changing in yield stress of metals, particularly steels, with good accuracy. AISI 4340 steel has the potential for being utilized in marine and submarine structures. The Johnson-Cook model relates flow stress to strain, strain rate, and temperature as follows [35]:

$$\sigma_y = \left(A + B\varepsilon_p^n\right)\left(1 + C\log\varepsilon_p^*\right)\left(1 - T_H^m\right), \tag{13}$$

where the coefficients A, B, C, n, and m are material constants specified for 4340 steel in Table 4 [35]. σ_y is flow stress, ε_p is the normalized plastic strain, ε_p^* is the normalized plastic strain rate, and T_H^m is the homogenized temperature which is defined by the following relation:

$$T_H^m = \frac{T - T_r}{T_m - T_r}, \tag{14}$$

where T_r is room temperature and T_m is melting temperature of the material.

4. Validity of the Implemented Numerical Scheme

As mentioned earlier, the validity of numerical simulations must be checked in every study and this can be performed in

Table 3: Polynomial EoS for water.

A_1 (GPa)	A_2 (GPa)	A_3 (GPa)	B_0	B_1	T_1	T_2	ρ (kg/m^3)
2.2	9.54	14.57	0.28	0.28	2.2	0	999

Table 4: Johnson-Cook properties of 4340 steel.

A (MPa)	B (MPa)	C	n	m	T_m (^{0}K)
792	510	0.014	0.26	1.03	1793

Table 5: Johnson-Cook constants of steel used in [2].

A (MPa)	B (MPa)	C	N	M	T_m (^{0}K)
217	233	0.07	0.643	1.03	1793

the best way if numerical results are compared with experimental ones. However, the specifications of available experimental results do not exactly match those of the present study. By increasing the size of the test, the amount of explosive material needs to be increased to create desirable deformations in the structure, and consequently more sophisticated and expensive instrumentation is needed. In this condition, generally, the accuracy of the test can be deteriorated. Hence, most of the experiments are conducted on scaled-down structures. In this paper, experimental results of [2] are chosen to validate the numerical results. Brett et al. [2], in a purely experimental study, investigated the response of steel cylindrical shells subjected to near-field underwater explosion. Cylindrical shell length, diameter, and thickness are 1200, 275, and 2 mm, respectively. Properties of mild steel used in [2] are provided in Table 5. PE-4 explosive charges are mounted at a 300 mm standoff distance from the cylinder outer surface and tests are carried out by 5 and 10 g charge weights. For making a comparison of experiments and numerical analysis of the present study, a full model [2] which contains the surrounding water and structures is set up in AUTODYN environment. Due to the symmetry of the problem, only one-quarter of the model is required to be modeled. Water medium is discretized by 168000 Eulerian cells and 2640 shell elements are implemented in the construction of one-quarter model of the cylinder. As reported in [2], the shell edges are restrained relatively rigidly, so the outer edges of the shell can be assumed to be perfectly clamped and the transmit boundary condition is applied on all of the outer planes of the Eulerian model to simulate a semidefinite medium without any wave reflection. To better perceive the detonation phenomenon using the remapping ability of AUTODYN, the explosion of a highly explosive material is modeled in 1D wedge environment and the results of one-dimensional simulation are mapped onto a 3D model after the shock wave's front reaches the vicinity of the nearest outer surface of the cylinder. This capability of AUTODYN can significantly help achieve highly accurate results where it may not be possible in the 3D model due to its tremendous numerical cost. Figure 3 illustrates a caption of the 3D model after the remapping process and when the shock front touches the cylindrical shell. Results of the present study using hydrocode simulation and [2] are tabulated in Table 6 for comparison.

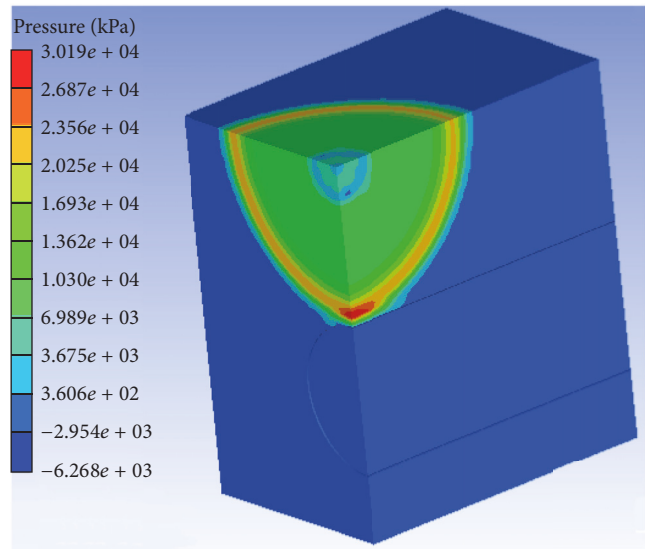

Figure 3: Three-dimensional model of the problem in [2] reconstructed in AUTODYN, a caption of pressure distribution as the shock front touches the shell.

Table 6: Results of experiment [2] and present hydrocode simulation. Central permanent deformation.

Test number	R (m)	W (g)	Experiment [2] (mm)	Present simulation (mm)
Event 2	0.3	5	7	5.95
Event 7	0.3	10	57.5	54.5

It is noteworthy that, in near-field explosions, prediction of structure response will be harder due to the interaction of bubbles and the structure. Considering this fact, the good agreement obtained between numerical and experimental results can be attributed to the complete modeling of detonation and shock propagation process and employing accurate numerical procedures; therefore, the employed numerical scheme would be a feasible tool for the anticipation of UNDEX loading on shell structures. Figure 4 depicts a view of the middle section of the cylinder deformed configuration for a 10 g charge weight where the correlation between simulated and measured values [2] can be observed.

5. Problem Description

5.1. Geometry of Target Cylindrical Shells. In this paper, four different cylinder configurations are studied. The cylinder length and diameter are 1000 and 300 mm, respectively, with 4 and 6.5 mm thicknesses. Moreover, two stiffening

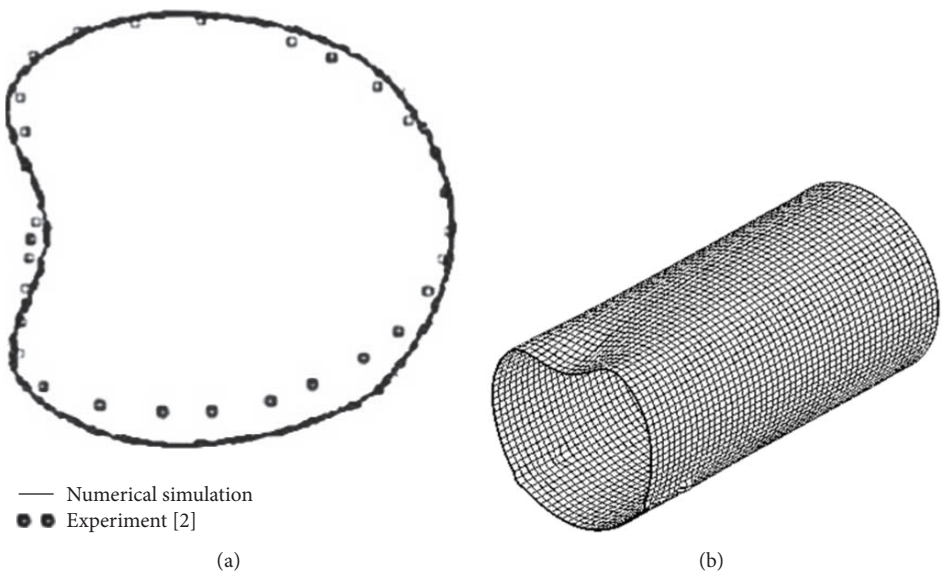

Figure 4: (a) Middle section of the cylindrical shell UNDEX blasted from the left side; comparison between the present numerical simulation and experiment [2]; (b) 3D caption, 10 g charge weight.

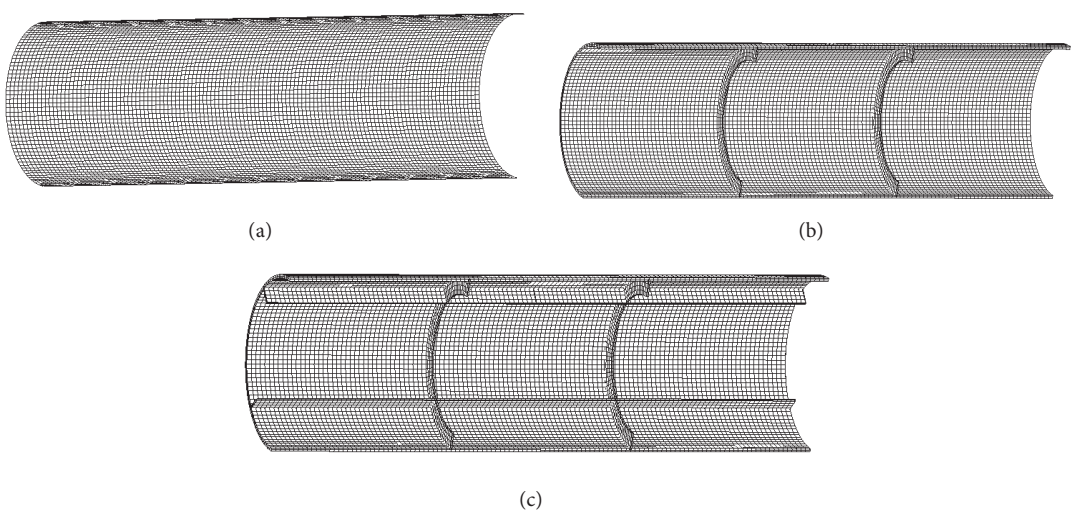

Figure 5: Cylindrical shells' geometrical presentation: (a) simple, (b) ring-stiffened, and (c) ring-longitudinal-stiffened cylindrical shell.

configurations are considered where rings and longitudinal stiffeners are utilized to reinforce the shell. The height of stiffeners is 30 mm and they have 4 mm thickness and are attached to the cylindrical shells with 6.5 mm thickness. Figure 5 illustrates the cylindrical shells considered here. Due to symmetry, half of the cylinders are shown.

5.2. Numerical Assessments. The general scheme for numerical modeling of UNDEX loading on cylinders is similar to what is described in Section 3. Here, further details of the numerical procedure are discussed. For every specific standoff distance, a distinct Eulerian grid is utilized for the discretization of the problem domain due to different distances from the center of the explosive charge to the outer diameter of cylinders. These Eulerian grids are fixed for all of the shell configurations. The number of Eulerian cells used for near (300 mm), medium (600 mm), and far (1000 mm) standoff distances is 112500 ($75 * 50 * 30$), 180000 ($50 * 30 * 120$), and 255000 ($50 * 30 * 170$), respectively, while 1600 ($40 * 40$) Lagrangian shell elements and 160 ($40 * 4$) elements for rings and longitudinal stiffeners (Figure 5) are implemented in the construction of simple cylindrical shell models. Meanwhile, validity analysis shows that an Eulerian grid with regular distribution is adequate for most remote UNDEX problems, whereas in powerful UNDEX cases very large deformations are probable and a finer grid should be used in the vicinity of the cylinder in order to better capture very large deflections and severe pressure gradients involved. Figure 6 illustrates a view of the aforementioned Eulerian grids. For every increment, the required mass of

Table 7: Incremental values of IMs for different configurations and different standoff distances.

Configuration	Standoff distance (mm)	$\Delta(1/Z)$	Configuration	Standoff distance (mm)	$\Delta(1/Z)$
Cylinder 4 mm	300	0.11	Cylinder 6.5 mm, ring-stiffened	300	0.13
	600	0.09		600	0.11
	1000	0.09		1000	0.11
Cylinder 6.5 mm	300	0.12	Cylinder 6.5 mm, ring- and longitudinal-stiffened	300	0.13
	600	0.11		600	0.12
	1000	0.11		1000	0.12

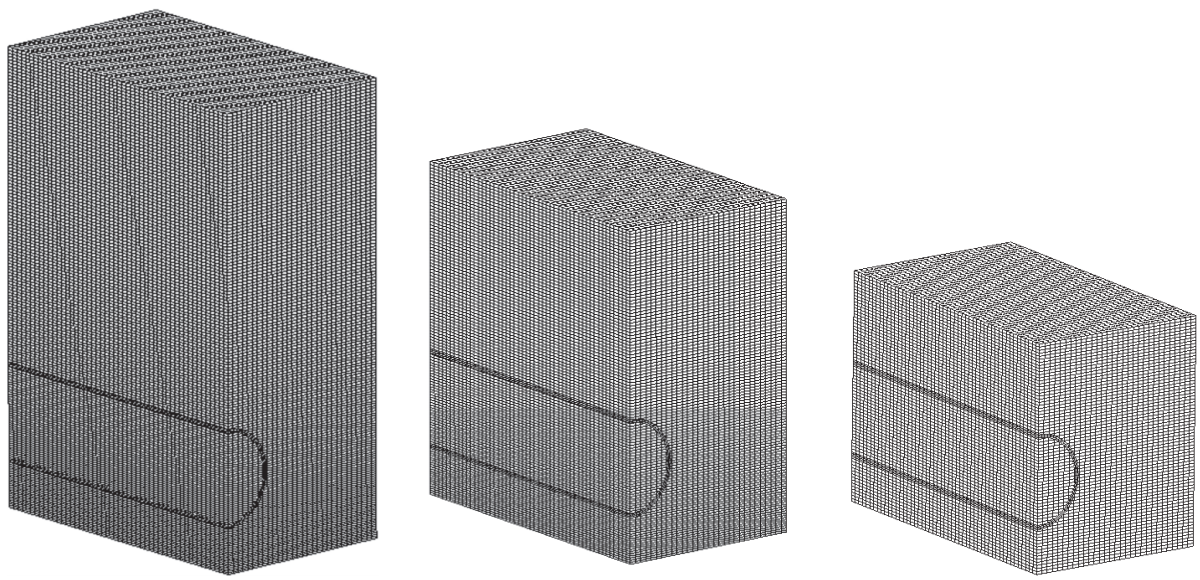

(a) (b) (c)

Figure 6: Eulerian grid for discretization of surrounding water medium: (a) far, (b) medium, and (c) near standoff explosion.

explosive is calculated, and according to the depth parameter, the internal energy of water is evaluated by means of (11). After constructing the finite element (FE) model for every configuration and for a particular (β, SD), the remapping process is performed to apply the outcomes of the simulated results of the 1D model onto the 3D model. Then, extensive simulations with the incremental IMs, mentioned in Table 7, are performed and the corresponding DMs are pinned to the IM-DM plane and the one-line IEA curve is built. Finally, for a specific configuration, that is, ring-stiffened cylindrical shell, the IEA curve is obtained as indicated in Figure 7.

6. Results and Discussion

Based on the method described in the preceding sections, numerical simulations are carried out and the corresponding results are outlined in this section. Figure 8 depicts deformed configuration of cylindrical shells for different configurations when a specific limit state happens.

After conducting numerous simulations, the IEA curves are extracted from the results. The incremental growth of $1/Z$ parameter is presented in Table 7. It should be noted that these incremental values are the maximum incremental values for every particular simulation. Figures 9 and 10 represent the IEA curves for all the configurations mentioned before. Different limit states are presented in Figures 9 and 10 versus the rotation angle (θ) and ductility ratio. Figures 9(a)–9(d) represent the IEA curves and the corresponding limit states observed in the analysis for the unstiffened cylindrical shells with 4 mm (a, b) and 6.5 mm (c, d) thickness under distinct loading conditions described as pairs of standoff distances and depth parameters (β, SD). As it can be seen, increasing the depth parameter results in larger θ's of the cylindrical shell for identical standoff distances. For instance, in Figure 9(a), increasing the depth parameter for standoff distance of 300 mm causes the curves to be shifted to the right, meaning that larger θ's are obtained. It is evident that the curves are very close to each other in the elastic portion of the deformation, just before the bay buckling state is reached, and become totally distinct when the nonlinear effects of plasticity dominate the deformation state. This emphasizes the necessity of implementing accurate models for representation of the material behavior. Comparison of Figures 9(a) and 9(c) indicates the effect of the enhanced strength of the material due to the greater thickness of the unstiffened shell. It can be observed that greater values of IM are required to obtain a particular value of θ for a cylindrical shell with 6.5 mm thickness. Increasing the shell thickness results in

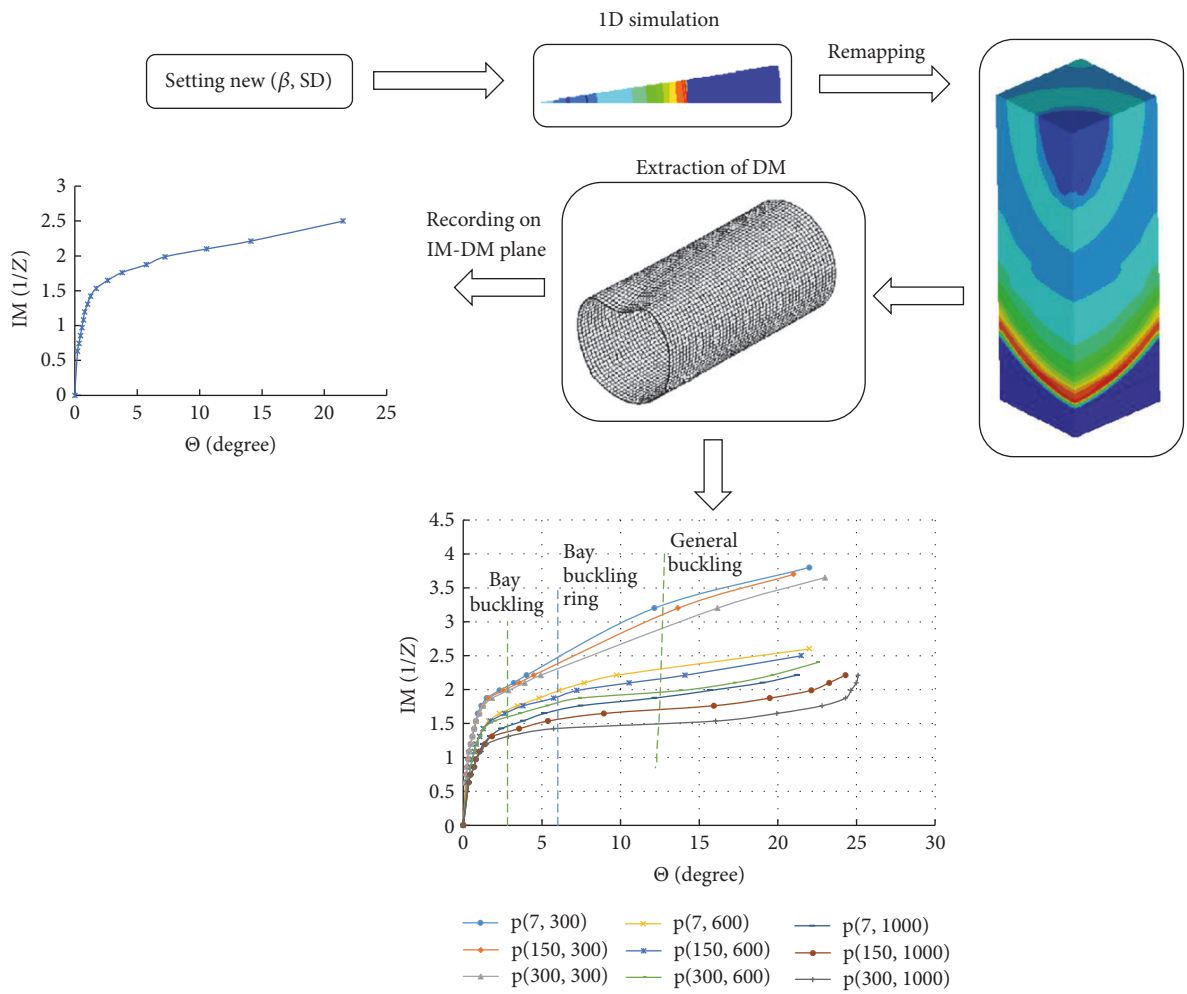

Figure 7: Schematic representation of the incremental explosive analysis (IEA) procedure.

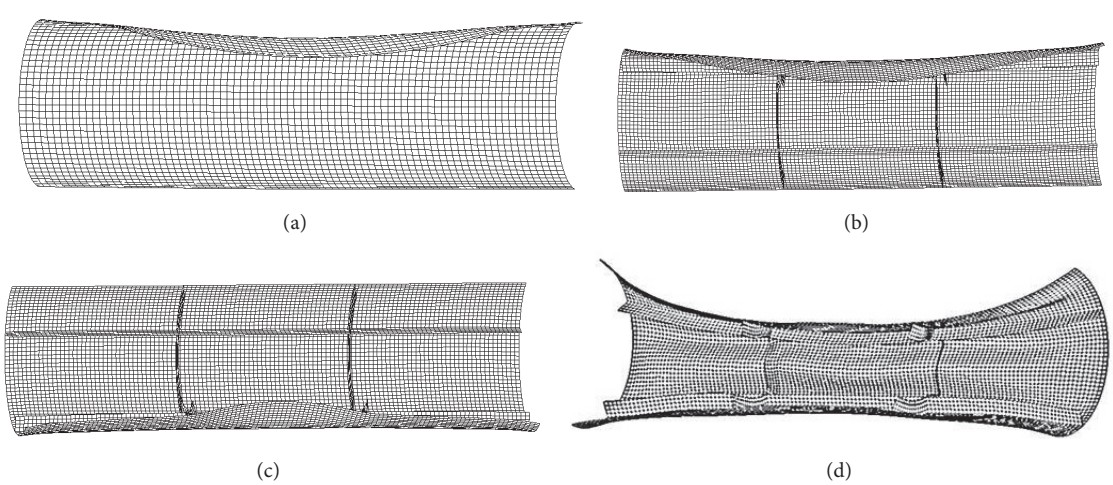

Figure 8: Deformed configuration of (a) bay buckling of unstiffened shell; (b) bay buckling of ring-stiffened cylinder; (c) local buckling of ring- and longitudinal-stiffened shell; (d) general buckling of ring- and longitudinal-stiffened shell at maximum DM. Only half of the shells are shown.

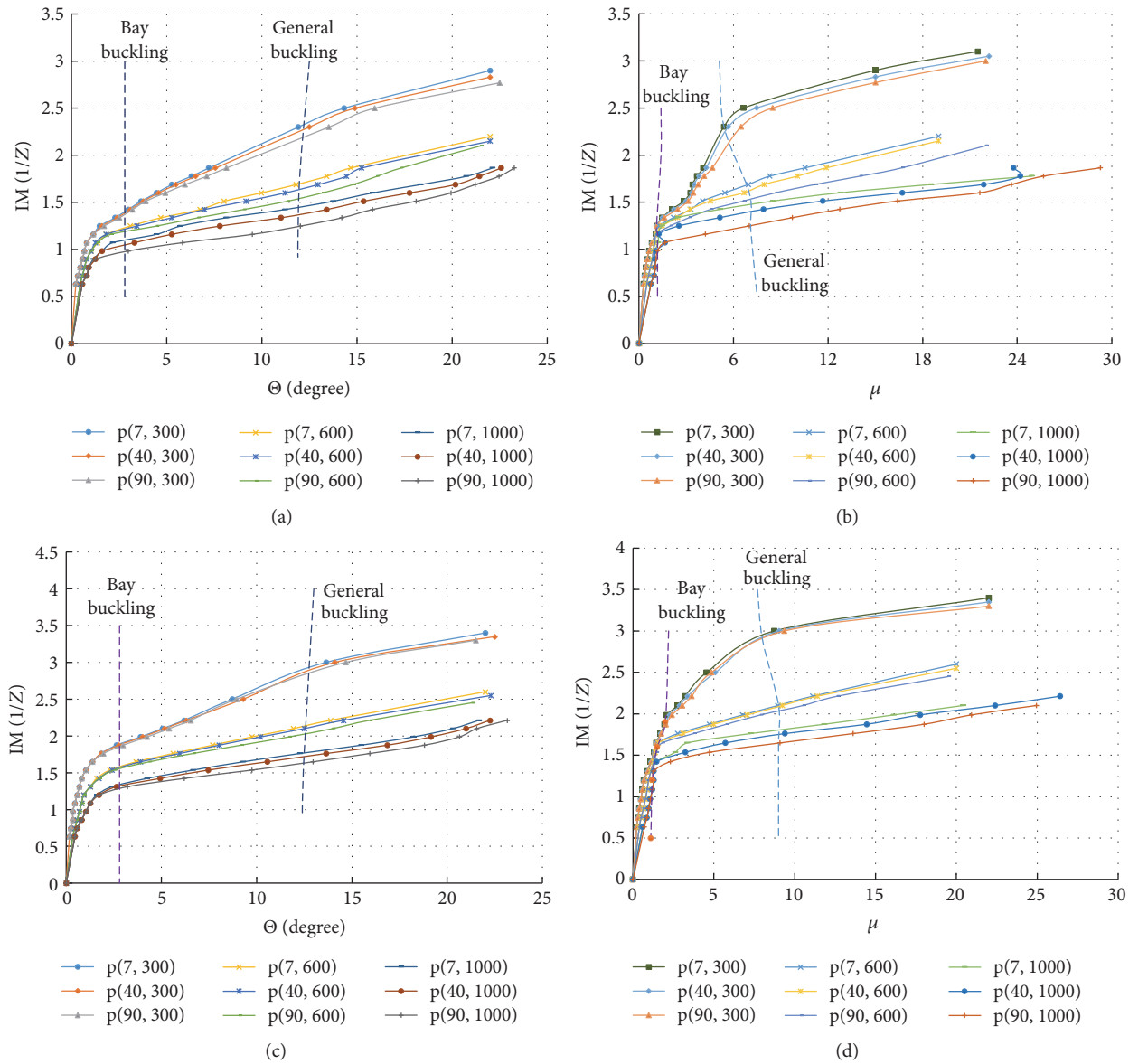

Figure 9: IEA curves obtained for unstiffened shell for all (β, SD)'s: 4 mm, (a) IM-θ and (b) IM-μ; 6.5 mm, (c) IM-θ and (d) IM-μ.

higher bending inertia and, consequently, greater resistance to the deformation rate. This also can be expressed as the higher θ value required to reach the general buckling limit state; the general buckling line in Figure 9(c) is shifted to the right in comparison to Figure 9(a). Increasing the thickness results in higher capacity of the cylindrical shell before it becomes totally unstable. A more definite difference may be found in the IM-μ diagrams represented in Figures 9(b) and 9(d). As discussed before, it is obvious that an increase in the depth parameter results in higher values of damage measurement μ. A very useful conclusion may be reached about the response of the cylindrical shell to the variation of depth parameter. As Figure 9 demonstrates, it is evident that increasing the standoff distance from 300 to 600 mm results in a very sharp decline in θ as well as μ.

On the other hand, imposing the ring stiffeners and combination of ring and longitudinal stiffeners makes the cylindrical shell firmer. Figures 10(a) and 10(b) represent the IEA curves for the ring-stiffened cylindrical shell for different loading conditions obtained from distinct depth parameter–standoff distance combinations. As discussed earlier, two equally spaced rings play the stiffening role in the analysis. It is evident that the increased rigidity of the structure resulted in lower deflections of the cylinder under equal loading conditions, that is, the same IM values. The effects of increasing depth parameter and standoff distance are identical to those discussed for the unstiffened cylindrical shells. As it can be seen from Figures 10(a) and 10(c) and comparing these two curves to Figures 9(a) and 9(c), the obtained θ for the general buckling limit state is very similar for all configurations and the difference between them emerges in the intensity measure of the conducted analysis as discussed before. Therefore, in order to better perceive the effect of stiffeners,

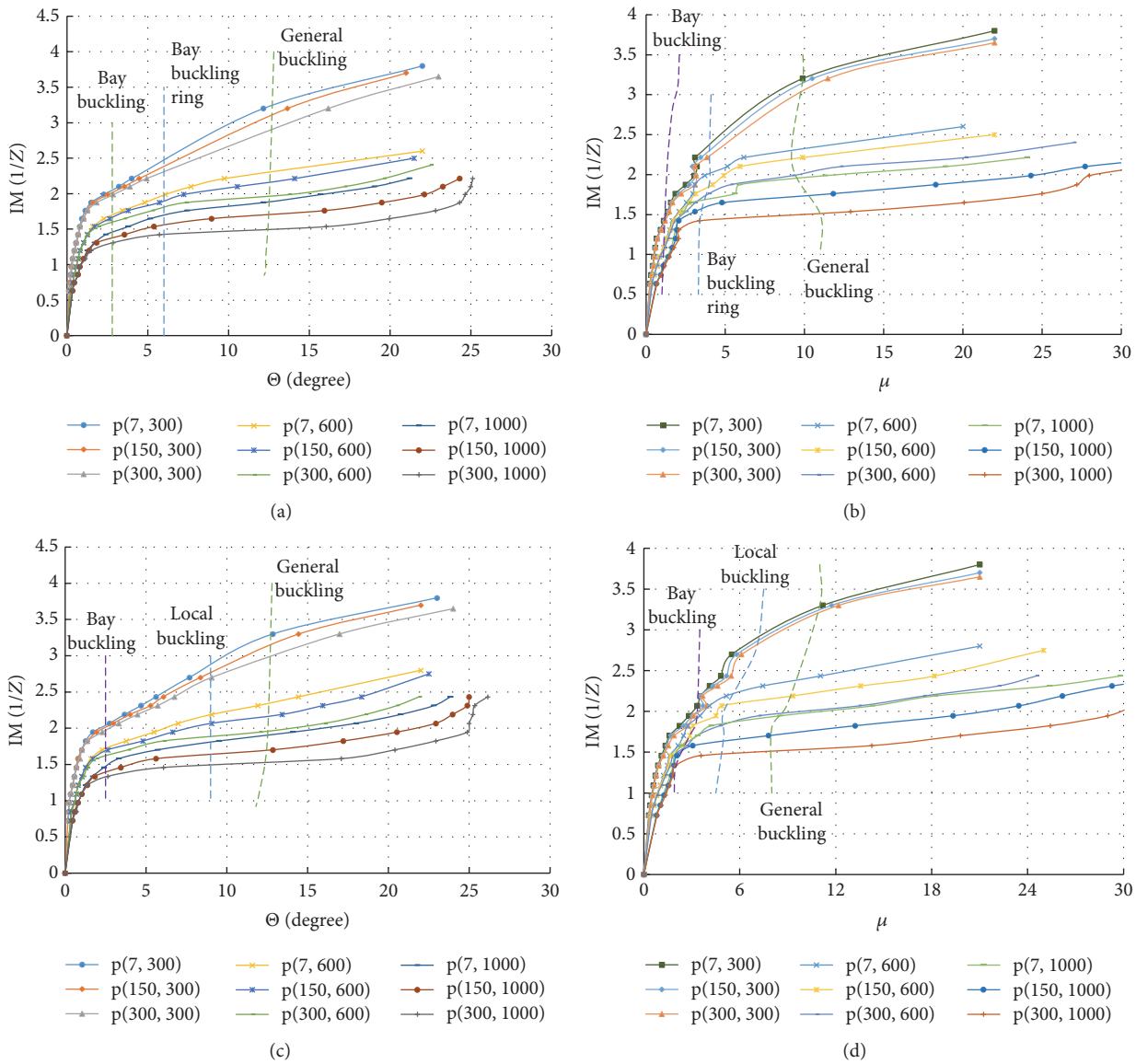

Figure 10: IEA curves obtained for ring-stiffened cylinder for all (β, SD)'s, (e) IM-θ and (f) IM-μ, and ring- and longitudinal-stiffened cylinder, (g) IM-θ and (h) IM-μ.

it is useful to consider the IM-μ represented in Figure 10. According to [35], the failure strain or the fracture strain (ε_f) of AISI 4340 is approximately 0.21. However, based on Figure 10(d), the maximum value recorded for μ is roughly 11 ($\mu = 11$). According to (4), it is concluded that the maximum equivalent strain of the stiffened shell reaches almost eleven times the elastic strain of AISI 4340; that would be $\varepsilon_M = 0.0242$. Comparing failure strain of the AISI 4340 with the obtained equivalent strain for the ring- and longitudinal-stiffened shell, which is considered the most firm configuration in the present study based on the IM-θ diagrams provided in Figure 10, it expands on this idea that the buckling instability comes before total failure of the material; here, the structure has reached the totally instable state, general buckling, in strains about eleven percent of the total failure strain of the material ($\varepsilon_M/\varepsilon_f \simeq 0.11$).

As it can be seen, different limit states such as the buckling modes are reached for different θ's and ductility ratios. The bay buckling mode was observed on the whole configurations as the first limit state that the cylindrical shell reaches. The corresponding θ for the bay buckling limit state is approximately 2.8° for all the configurations. It should be noticed that the ductility ratio is not constant through the analysis and follows an incremental growth at higher intensity measures. It should be mentioned that the bay buckling and general buckling have occurred in all configurations, while the general buckling does not yield a particular and constant θ as the bay bucking does. It takes the form of an incremental growth in θ with increasing intensity measure. But the corresponding line for the general buckling demonstrates semigrowth and decline in the values of ductility ratio with increasing intensity measure. As illustrated in Figure 10, the

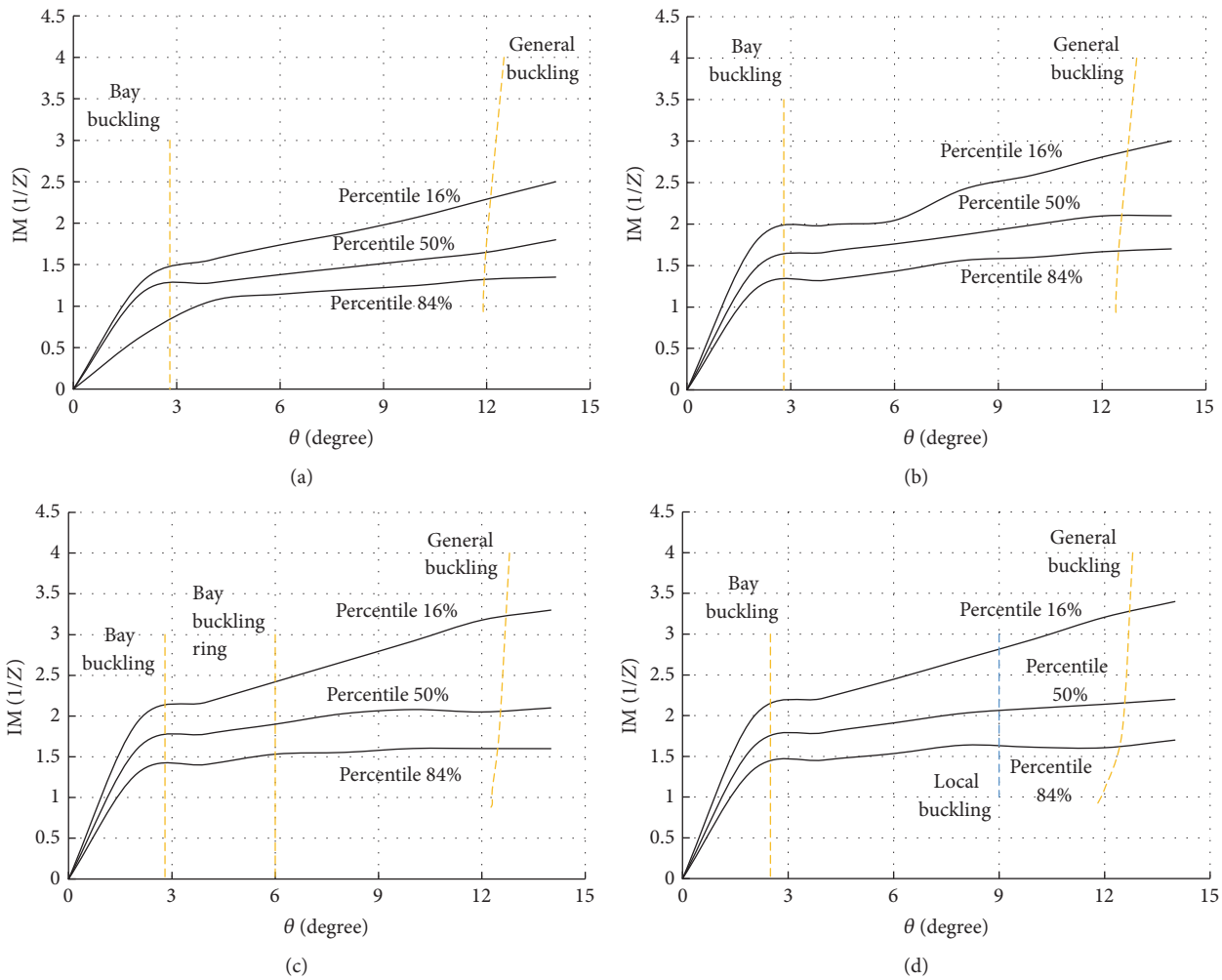

Figure 11: IEA curves of four different configurations with three percentiles including distinct limit states: (a) unstiffened shell, 4 mm; (b) unstiffened shell, 6.5 mm; (c) ring-stiffened shell, 6.5 mm; and (d) ring- and longitudinal-stiffened shell, 6.5 mm.

local buckling state was only observed in the cylindrical shell stiffened with ring and longitudinal stiffeners and appears between the two other limit states, that is, bay buckling and general buckling limit states. This phenomenon emphasizes the importance of studying different configurations with distinct stiffening arrangements. Similarly, the bay buckling of the rings has also appeared just in the ring-stiffened configuration that contains greater values of θ and ductility ratio. Since there are numerous parameters that affect the response of the shell structure to UNDEX phenomenon, there should be a statistical analysis to show the probability of the induced damage in the structure. Therefore, the IEA curves have to be summarized to better show the survival rate of the structure under different loading conditions. In the present study, the method of fractiles (based on the normal distribution of the obtained data) has been employed based on the maximum shell's edge rotation (θ) as a DM parameter. Figure 11 depicts the IEA curves of the four different configurations with these percentiles alongside the corresponding limit states. As discussed in Section 2.2, different limit states are considered for the evaluation of the structural performance during the incremental loading. Bay buckling limit state was reached in all four different configurations, corresponding to approximately constant $\theta = 2.8^\circ$ according to the various FE analyses conducted in the present study. General limit state is also noticed in all four configurations, corresponding to variable θ with respect to the IM value in the distinct structural configurations as demonstrated in Figure 11. Finally, local buckling is also observed for the cylindrical shell stiffened with ring and longitudinal stiffeners, corresponding to $\theta = 9^\circ$ (constant). This method summarized the results of analysis into their 16%, 50%, and 84% fractile. These three percentiles are chosen based on the normal distribution of the obtained values. According to Figure 11(a), for the acquired IM $(1/Z) = 1.0$, 16% of explosions yield $\theta \leq 1.5^\circ$, 50% of them result in $\theta \leq 1.75^\circ$, and 84% of detonations produce $\theta \leq 3.8^\circ$, approximately. As the thickness of the shell increases from 4 mm to 6.5 mm, the acquired IM $(1/Z) = 1.0$ values result in smaller values of θ since the bending strength of the unstiffened cylindrical shell increases significantly. According to Figure 11, bay buckling limit state has been reached for higher values of

IM in Figure 11(b) in comparison with Figure 11(a), implying that the unstiffened cylindrical shell with greater thickness can sustain higher magnitude of incoming shock wave generated from UNDEX. Higher values of $1/Z$ result in higher strain rates and, according to the Johnson-Cook structural model, lead to higher failure stresses. General buckling limit state as the completely unstable situation of the structure is also reached for higher values of IM for a shell with 6.5 mm thickness (Figure 11(b)) in comparison to the shell with 4 mm thickness (Figure 11(a)). In addition, the general buckling limit state was observed for higher corresponding θ's. Figure 11(c) represents the summarized IEA curve with the different limit states and fractile percentages for a ring-stiffened cylindrical shell with 6.5 mm thickness. Similar to the thickness effect, the added rings also have a strengthening effect and further reinforce the structure. Furthermore, bay buckling of the ring was also observed in the analysis for $\theta = 6^\circ$ (constant) which happened after bay buckling of the shell itself. At the end, Figure 11(d) also demonstrates the summarized IEA curves of the ring and longitudinal-stiffened cylindrical shell with bay, local, and general buckling limit states which were observed in the analysis. The comparison of Figures 11(c) and 11(d) shows in an obvious manner the strengthening effects of the longitudinal stiffeners. Adding these stiffeners has also made the local buckling of the cylindrical shell possible. However, the longitudinal stiffeners affect the summarized IEA curves more significantly at θ's lower than that of bay buckling, that is, $\theta = 2.8^\circ$.

In addition, another useful and more convenient tool for designers who deal with design and assessment of marine structures subjected to probabilistic loadings is fragility curves [26]. After performing preliminary analysis to attain the IEA data, the fragility curves can be extracted to anticipate whether the structure has exceeded a certain limit state such as general buckling limit state or the occurrence of multiple buckling mode. Considering the fact that the IEA data follow a normal distribution, it is practical to derive the fragility curves for a specific limit state. In order to obtain these curves for the IEAs provided and discussed earlier, the normal logarithm curve is employed and the Error Function or Gauss Error Function is obtained by the following equations [36]:

$$\mu^* = \log\left(\frac{m^{*^2}}{\sqrt{v + m^{*^2}}}\right) \tag{15}$$

$$\sigma^* = \sqrt{\log\left(v + m^{*^2} + 1\right)} \tag{16}$$

$$y = f\left(x, \mu^*, \sigma^*\right) = \frac{1}{x\sigma^*\sqrt{2\pi}} e^{-(\ln(x)-\mu^*)/2\sigma^{*2}} \tag{17}$$

$$Y = \frac{1}{2} + \frac{1}{2}\operatorname{erf}\left[\frac{\ln(x) - \mu^*}{\sigma^*\sqrt{2}}\right], \tag{18}$$

where m^*, v, μ^*, and σ^* are the average, the variance, the location parameter, and the scale parameter of the IEA data, respectively. The parameter y refers to the probability density function of occurrence x and Y stands for accumulative distribution function which is drawn in Figure 11. Figure 12 shows the fragility analysis conducted on the different configurations of cylindrical shells: the probability (percentile) of exceeding the certain limit state with respect to IM ($1/Z$) value obtained from IEA. Figure 12 provides useful information about the possibilities of instability of the shell under different operational conditions. It is perceived that the probability of bay buckling limit state occurrence is changed drastically from zero to one in all configurations for specific and distinct values of IMs. For instance, for an unstiffened shell with 4 mm thickness (Figure 12(a)), the bay buckling occurrence probability is equal to zero when IM = 1.17 and suddenly reaches one when IM = 1.25, approximately. Again, increasing the shell thickness (Figure 12(b)) and the different stiffening methods (Figures 12(c) and 12(d)) cause the structure to reach a specific limit state for higher IM values. For example, the IM is approximately 1.63, 1.75, and 1.75 for Figures 12(b), 12(c), and 12(d), respectively. It is observed that, for small incremental values of IM, the occurrence probability of bay buckling limit state is changed from zero to one. On the other hand, the occurrence probability of general buckling limit state follows a much smoother pattern and requires more growth in IM in comparison to the bay buckling limit state. The strengthening effect of the reinforcements is also distinguished between different configurations. As it can be seen, the general buckling and bay buckling limit states have no common occurrence and are completely separated from each other. However, in both Figures 12(c) and 12(d), for identical IMs, multiple buckling modes are observed. For instance, when IM is equal to 2.0 in Figure 12(c), the approximate occurrence probability of ring bay buckling and general buckling is 90% and 10%, respectively. Similarly, in Figure 12(d), when IM = 2.25, the approximate occurrence probability of local buckling and general buckling becomes 85% and 43%, respectively.

7. Conclusions

In this study, the incremental explosive analysis is established for performance-based assessment of stiffened and unstiffened cylindrical shells subjected to UNDEX. Since this approach gains its advantages generally from the incremental dynamic analysis, the proposed methodology is called incremental explosive analysis. The performance of structures, which are intended to be explosion resistant, can be evaluated by IEA considering the uncertain nature of explosive loading. Both demand and capacity of structures were addressed by IEA. Rigorous analysis led to the production of the multi-IEA curves as representing the shells' responses. The statistical treatment of the obtained IEA curves was performed in order to summarize the results and to use them effectively in a predictive mode. The variability and vagaries of a nonlinear structural system under UNDEX loads lead to the need for this treatment. The standoff distance and depth parameter that influence UNDEX loading and its uncertain character were chosen for this primary study. In addition, the fragility curves were extracted from data that were obtained from IEA. The use of IEA approach can be generalized for other fields of blast engineering such as underground and in-air explosions by their special considerations.

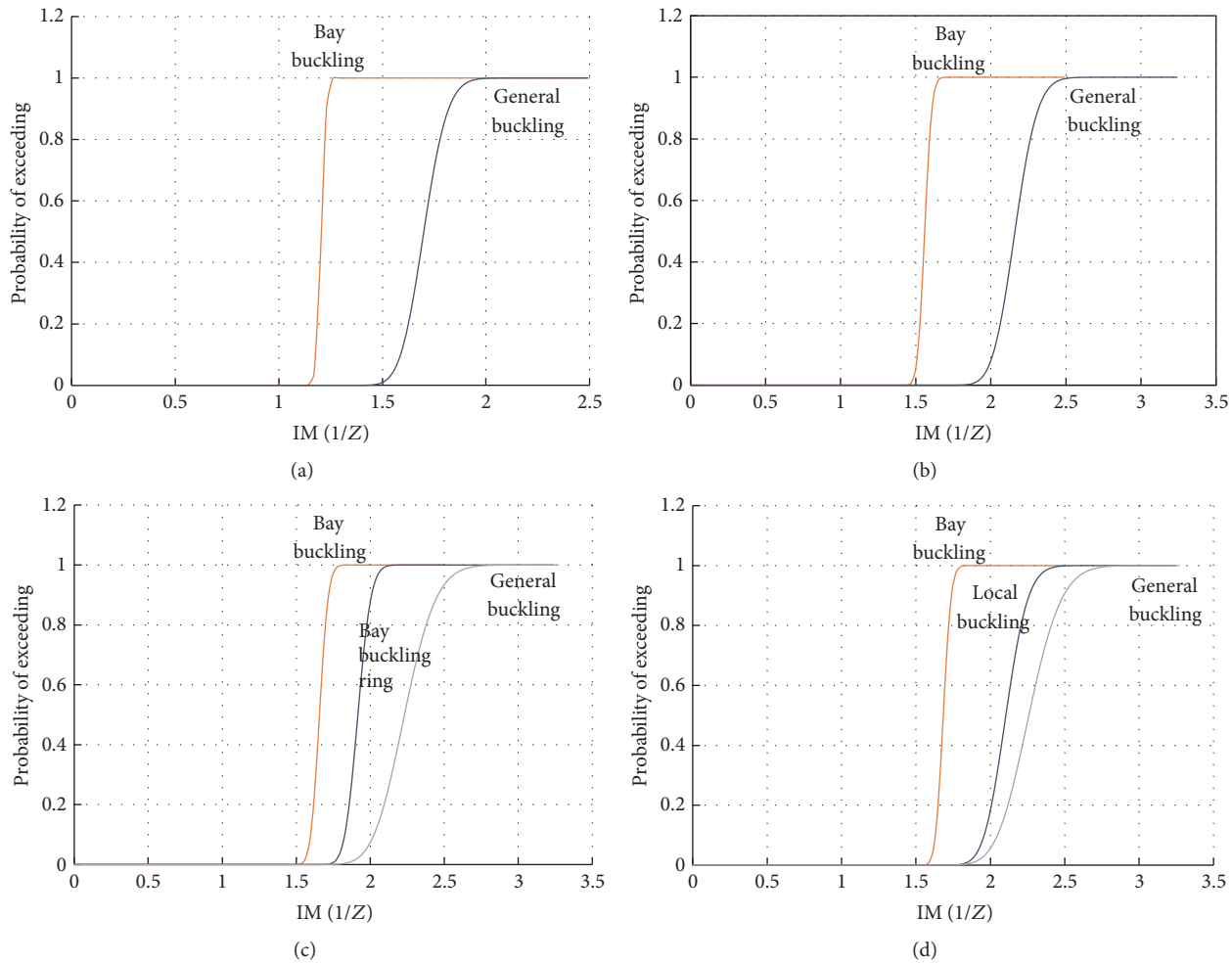

Figure 12: Fragility curves of cylindrical shells with distinct limit states: (a) unstiffened shell, 4 mm; (b) unstiffened shell, 6.5 mm; (c) ring-stiffened shell, 6.5 mm; and (d) ring- and longitudinal-stiffened shell, 6.5 mm.

The most important results of the present study can be outlined as follows:

(i) The IEA method is an advantageous method to derive the structural performance in the whole range of stable and unstable states of the structure and to demonstrate the structural capacity in a more sensible and comprehensible way.

(ii) The bay buckling limit state has been reached almost for all configurations and for approximately identical rotation of the shell's edge based on the derived IEAs. The general buckling also was observed in all configurations but with different critical values of θ. The corresponding line that represents the general buckling limit states on the IEA curves has a growth and decline pattern, implying that the final unstable state of every configuration is affected by the major parameters of the process, that is, standoff distance and depth parameter. As such, it is essential to treat these two parameters with care.

(iii) According to the IEA curves, studying different configurations provided very good knowledge about distinct possible damage causes that stiffened and unstiffened cylindrical shells may undergo. As illustrated, the local buckling mode emerged in the cylindrical shell stiffened with transverse rings and longitudinal stiffeners. On the other hand, the bay buckling of the rings is observed in the ring-stiffened configuration.

(iv) According to IEA curves, increasing of the depth parameter results in larger θ_s and μ_s of the cylindrical shell for identical standoff distances. In addition, increasing the standoff distance leads to an abrupt decline in θ as well as μ.

(v) Stiffeners are more effective in farther standoffs due to the global deformation of the structure, while in nearer standoffs local loading reduces the effective functioning of stiffeners.

(vi) Summarization of IEA curves and constructing the fragility curves result in a concise presentation of data

which can assist designers for a better performance-based design of structures against various levels of UNDEX threats.

Finally, it is noteworthy that several studies have reported that there is a moderate imperfection sensitivity in lateral pressure loading on cylindrical shells which may have an effect on the accurate bay buckling load estimation. However, in the present study, this aspect of structural uncertainty is not considered for the sake of avoiding complicated interaction with UNDEX loading uncertainties. As a suggestion, this aspect of uncertainty can be addressed in future researches.

Conflicts of Interest

The authors declare that there are no conflicts of interest regarding the publication of this article.

References

[1] Y. Kwon and P. Fox, "Underwater shock response of a cylinder subjected to a side-on explosion," *Computers & Structures*, vol. 48, pp. 637–646, 1993.

[2] J. M. Brett, G. Yiannakopoulos, and P. J. van der Schaaf, "Time-resolved measurement of the deformation of submerged cylinders subjected to loading from a nearby explosion," *International Journal of Impact Engineering*, vol. 24, no. 9, pp. 875–890, 2000.

[3] K. Ramajeyathilagam, C. P. Vendhan, and V. Bhujanga Rao, "Experimental and numerical investigations on deformation of cylindrical shell panels to underwater explosion," *Shock and Vibration*, vol. 8, no. 5, Article ID 798735, pp. 253–270, 2001.

[4] W. Zhang and H. Yang, "A study of the weighting method for a certain type of multicriteria optimization problem," *Computers & Structures*, vol. 79, no. 31, pp. 1635–1644, 2001.

[5] L. A. Gish, *Analytic and numerical study of underwater implosion*, Massachusetts Institute of Technology, 2013.

[6] C. Y. Hsu, T. L. Teng, C. C. Liang, H. A. Nguyen, and C. J. Shih, "The study on the dynamic response of cylindrical pressure hull on the different shock loading empirical formula," *Applied Mechanics and Materials*, vol. 799-800, pp. 604–609, 2015.

[7] C. F. Hung, B. J. Lin, J. J. Hwang-Fuu, and P. Y. Hsu, "Dynamic response of cylindrical shell structures subjected to underwater explosion," *Ocean Engineering*, vol. 36, no. 8, pp. 564–577, 2009.

[8] W. Xiao, A. M. Zhang, and S. P. Wang, "The whipping response of a fluid filled cylindrical shell subjected to an underwater explosion," *Marine Structures*, vol. 52, pp. 82–93, 2017.

[9] Y.-J. Lee, C.-H. Hsu, and C.-H. Huang, "Pressure hull analysis under shock loading," *Shock and Vibration*, vol. 15, no. 1, pp. 19–32, 2008.

[10] C. Y. Jen, "Coupled acoustic-structural response of optimized ring-stiffened hull for scaled down submerged vehicle subject to underwater explosion," *Theoretical and Applied Fracture Mechanics*, vol. 52, no. 2, pp. 96–110, 2009.

[11] S. Gupta, H. Matos, J. M. Leblanc, and A. Shukla, "Shock initiated instabilities in underwater cylindrical structures," *Journal of the Mechanics and Physics of Solids*, vol. 95, pp. 188–212, 2016.

[12] C. Yin, Z. Jin, Y. Chen, and H. Hua, "Shock mitigation effects of cellular cladding on submersible hull subjected to deep underwater explosion," *Ocean Engineering*, vol. 117, pp. 221–237, 2016.

[13] J. Li and J.-L. Rong, "Experimental and numerical investigation of the dynamic response of structures subjected to underwater explosion," *European Journal of Mechanics - B/Fluids*, vol. 32, no. 1, pp. 59–69, 2012.

[14] Y. S. Shin and D. T. Hooker, "Damage response of submerged imperfect cylindrical structures to underwater explosion," *Computers & Structures*, vol. 60, no. 5, pp. 683–693, 1996.

[15] X.-L. Yao, J. Guo, L.-H. Feng, and A.-M. Zhang, "Comparability research on impulsive response of double stiffened cylindrical shells subjected to underwater explosion," *International Journal of Impact Engineering*, vol. 36, no. 5, pp. 754–762, 2009.

[16] W. Zhang and W. Jiang, "An improved shock factor to evaluate the shock environment of small-sized structures subjected to underwater explosion," *Shock and Vibration*, vol. 2015, Article ID 451583, 2015.

[17] J. Yuan and X. Zhu, "Dynamic response of a ring-stiffened cylindrical shell subjected to underwater explosive loading," *Applied Mechanics and Materials*, vol. 105-107, pp. 931–936, 2012.

[18] D. Vamvatsikos and C. A. Cornell, "Applied incremental dynamic analysis," *Earthquake Spectra*, vol. 20, no. 2, pp. 523–553, 2004.

[19] A. Zacharenaki, M. Fragiadakis, D. Assimaki, and M. Papadrakakis, "Bias assessment in incremental dynamic analysis due to record scaling," *Soil Dynamics and Earthquake Engineering*, vol. 67, pp. 158–168, 2014.

[20] M. Alembagheri and M. Ghaemian, "Damage assessment of a concrete arch dam through nonlinear incremental dynamic analysis," *Soil Dynamics and Earthquake Engineering*, vol. 44, pp. 127–137, 2013.

[21] D. Vamvatsikos and C. A. Cornell, "Incremental dynamic analysis," *Earthquake Engineering & Structural Dynamics*, vol. 31, no. 3, pp. 491–514, 2002.

[22] A. Ajamy, M. R. Zolfaghari, B. Asgarian, and C. E. Ventura, "Probabilistic seismic analysis of offshore platforms incorporating uncertainty in soil-pile-structure interactions," *Journal of Constructional Steel Research*, vol. 101, pp. 265–279, 2014.

[23] P. Tehrani and D. Mitchell, "eismic performance assessment of bridges in Montreal using incremental dynamic analysis," in *Proceedings of the 15th World Conf on Earthquake Engineering*, 2012.

[24] B. Asgarian and A. Ajamy, "Seismic performance of jacket type offshore platforms through incremental dynamic analysis," *Journal of Offshore Mechanics and Arctic Engineering*, vol. 132, no. 3, Article ID 031301, 2010.

[25] M. R. Zolfaghari, A. Ajamy, and B. Asgarian, "A simplified method in comparison with comprehensive interaction incremental dynamic analysis to assess seismic performance of jacket-type offshore platforms," *International Journal of Advanced Structural Engineering*, vol. 7, no. 4, pp. 353–364, 2015.

[26] I. Mansouri, G. Ghodrati Amiri, J. W. Hu, M. Khoshkalam, S. Soori, and S. Shahbazi, "Seismic Fragility Estimates of LRB Base Isolated Frames Using Performance-Based Design," *Shock and Vibration*, vol. 2017, pp. 1–20, 2017.

[27] A. A. Golafshani, V. Bagheri, H. Ebrahimian, and T. Holmas, "Incremental wave analysis and its application to performance-based assessment of jacket platforms," *Journal of Constructional Steel Research*, vol. 67, no. 10, pp. 1649–1657, 2011.

[28] M. Zeinoddini, H. Matin Nikoo, and H. Estekanchi, "Endurance Wave Analysis (EWA) and its application for assessment of offshore structures under extreme waves," *Applied Ocean Research*, vol. 37, pp. 98–110, 2012.

[29] R. H. Cole, "Underwater explosions," 1984.

[30] R. Rajendran and K. Narasimhan, "Performance evaluation of HSLA steel subjected to underwater explosion," *Journal of Materials Engineering and Performance*, vol. 10, no. 1, pp. 66–74, 2001.

[31] B. Le Méhauté and S. Wang, "Water waves generated by underwater explosion," *World Scientific*, 1996.

[32] A. Shipping, *Guide for buckling and ultimate strength assessment for offshore structures*, ABS Plaza, New York, NY, USA, 2014.

[33] D. Vamvatsikos and C. Allin Cornell, "Incremental dynamic analysis," *Earthquake Engineering & Structural Dynamics*, vol. 31, no. 3, pp. 491–514, 2002.

[34] G. Wang, S. Zhang, M. Yu, H. Li, and Y. Kong, "Investigation of the shock wave propagation characteristics and cavitation effects of underwater explosion near boundaries," *Applied Ocean Research*, vol. 46, pp. 40–53, 2014.

[35] T. Autodyn, *Theory Manual Revision 4.3*, Century Dynamics. Inc, Concord, CA, USA, 2003.

[36] W. Feller, *An Introduction to Probability Theory and ITS Applications*, John Wiley & Sons, 2008.